[39]A. C. Riviere, Atomic Energy Research Establishment, Harwell, Berkshire, U.K. Report No. AERE-R-4818, 1964 (unpublished), pp. 124–135.

[40]K. H. Berkner, L. Kay, and A. C. Riviere, Nucl. Fusion 7, 29 (1967).

[41]It has been pointed out by Butler and May [S. T. Butler and R. M. May, Phys. Rev. 137, A10 (1965)] that ionization of a highly excited level by collisions with atoms should be independent of $n$.

[42]P. M. Stier and C. F. Barnett, Phys. Rev. 103, 896 (1956).

[43]S. V. Bobashev, V. A. Ankudinov, and E. P. Andreev, Zh. Eksperim. i Teor. Fiz. 48, 833 (1965) [English transl.: Soviet Phys. – JETP 21, 554 (1965)].

[44]The ordering is obtained from G. Lüders, Ann. Physik 8, 301 (1951). The method of presenting the ordering follows that used for the $n=7$ level by A. C. Riviere, Culham Report No. CLM-M23, 1963 (unpublished), Fig. 5.

PHYSICAL REVIEW VOLUME 182, NUMBER 1 5 JUNE 1969

# Measurement of the Total Cross Section for Charge Transfer into the Metastable State H(2$s$) for Protons Incident on $H_2$ and Ar Gases*

James E. Bayfield

*Gibbs Laboratory, Yale University, New Haven, Connecticut* 06520

(Received 17 February 1969)

The energy dependence of the total cross section for $H^+ + H_2 \rightarrow H(2s) + H_2^+$ exhibits two broad maxima in the range 2–70 keV. The lower maximum occurs at an energy where the total charge-transfer cross section is largest, and thus may be due to coupling with the ground-state scattering channel. The observed energy dependence is similar to that for $H^+ + H_2 \rightarrow$ Ly $\alpha$, but with the positions of both maxima shifted to higher energies by about 5 keV. The cross section for $H^+ + Ar \rightarrow H(2s) + Ar^+$ over the extended energy range 2–70 keV also exhibits only two maxima. Internal and external quenching measurements of this cross section are in agreement. Its absolute magnitude at 20 keV has now been independently measured by three investigators, with results consistent with ± 20%.

## I. INTRODUCTION

The measurement of atomic collision cross sections basically involves the determination of three quantities: The incident beam intensity, the thickness of the scattering target, and the scattered beam intensity. In the study of the electron or charge transfer process $H^+ + X \rightarrow H + X^+$ at keV energies, fast hydrogen atoms produced in the scattering can be separated from elastically scattered protons by an electric or magnetic deflection field. The study of charge transfer into an excited state H($nl$) necessitates additional state-sensitive detection of a portion of the scattered atom beam.

The metastable H(2$s$) atom component of a fast hydrogen-atom beam can be selectively detected through induced decay. An external dc electric field applied to the beam couples the long-lived 2$s$ state with the nearby short-lived 2$p$ state. At sufficiently high fields the mixed state has a short lifetime and decays to the ground state within the field region. This Stark-effect quenching of metastable atoms therefore results in the emission of Lyman-alpha (Ly-$\alpha$) photons; an intensity measurement of this radiation determines the intensity of the metastable atom beam.

The direct study of charge transfer into H(2$s$) was first undertaken by Madansky and Owen[1] using a 10-keV proton beam and an $H_2$ gas-scattering target. It was known that charge transfer would occur at relatively large impact parameters, and that atomic scattering at keV energies is approximately controlled by the screened Coulomb potential. Thus an "external-quenching" type of experiment was performed, in which fast H(2$s$) atoms were searched for outside the scattering cell, within a small solid angle centered around the direction of the incident beam. This experimental approach to measuring the cross section $\sigma_{2s}(H_2)$ for the $H^+ + H_2$ system has been used by several investigators studying differing energy ranges.[2–4]

Measurements of $\sigma_{2s}$ have also been made for protons incident on inert-gas targets.[5–7] Argon scattering targets were used by Jaecks, Van Zyl,

and Geballe[5] in studies covering the energy range 1.5 to 23 keV, and by Andreev, Ankudinov, and Bobashev[6] for energies between 10 and 40 keV. These experiments differed in nature from the external-quenching experiments done with $H_2$ in that the fast H(2*s*) were quenched and observed while inside the scattering target. Such studies may be called "internal-quenching" experiments.

The two types of experiment have different limitations. The principal problem associated with external quenching lies in the transmission of *all* scattered fast H(2*s*) atoms from the scattering target to the detection region. Difficulties with insufficient solid-angle acceptance or premature quenching by stray electric fields may explain some of the large discrepancies that presently exist in the data for $H_2$.[2,3]

The internal-quenching technique is usable only when the desired Ly $\alpha$ radiation can be separated from radiation produced by excitation of target molecules. This limitation makes studies of $H^+ + H_2$ difficult, for many lines of $H_2$ lie close to the Ly $\alpha$ wavelength of 1216 Å. Previous investigators have not found this to be a problem for the inert gases.

One of the uncertainties inherent in internal-quenching experiments is the perturbation of the incident proton energy by the relatively large quenching field. Also, there is the possibility that the field affects the cross section itself, either directly or through the cascade contribution arising from higher excited-state production.

The external-quenching method was chosen for the present measurements. Complete collection of fast H(2*s*) was verified through studies of the angular distribution at small angles. The present studies of $H^+ + Ar$ make possible the comparison of results for the two quenching methods. The energy range selected for study (2 to 70 keV) was large enough to overlap and extend all earlier data.

Absolute values for the cross section $\sigma_{2s}(Ar)$ are of special interest because it remains large ($\gtrsim 0.1$ Å$^2$) down to at least 1 keV. Argon gas, therefore, is especially useful as a reference target in the measurement of cross-section ratios.[8]

## II. APPARATUS

### A. General Description

A schematic diagram of the apparatus as viewed from above is shown in Fig. 1. A hydrogen-ion beam was extracted from a radio-frequency discharge and then accelerated to the desired energy. After electrostatic positioning, the beam was magnetically mass-analyzed and collimated by two small apertures a large distance apart. The beam then passed into a differentially pumped scattering cell containing the target gas. Fast scattered and unscattered beam particles left the target region through a vertical tapered rectangular channel. The incident proton beam passing through the cell could be electrostatically deflected into a Faraday-cup assembly.

When actual cross-section measurements were being made, the entire beam was passed through a long drift region, where all charged beam particles were deflected slightly onto slit surfaces. The ion removal field in the drift region was designed to minimize the quenching of metastable atoms in the beam. The neutral atom beam produced in the scattering target traveled to the end of the apparatus where its intensity and metastable-atom content were measured. The latter was determined by means of electrostatic quenching and Ly-$\alpha$ counting. A magnetic vacuum-ultraviolet photomultiplier was used as the Ly-$\alpha$ detector. After passing through the H(2*s*) quench region, the neutral atom beam was monitored through the emission of secondary electrons from a beam-stopping plate. Both the H(2*s*) and total neutral-atom detection devices were mounted on a vertical-motion translator so that angular distributions could be studied.

Scattering target densities were determined in two ways. One method used measurements of target gas flow in conjunction with conductance calculations. The other method involved the detection of neutral atoms and the use of known charge-transfer cross sections $\sigma_{10}$ at the higher energies.

The experiment was performed inside a bakeable vacuum system equipped with mercury diffusion pumps. Figure 1 shows the positions of differential pumping conductances that were placed between separately pumped regions of the vacuum system. The pressure inside the apparatus, with ion source and target gas flows off, was usually about $3\times10^{-9}$ Torr. Differential pumping produced detector chamber pressures a factor of $10^4$ to $10^5$ less than the scattering target pressure.

### B. The Proton Beam

The ion source was a commercially available version of the Thoneman radio-frequency discharge source[9] (ORTEC Model 320). Extraction voltages of 1 to 3 kV were used. An axial magnetic field was applied to the source discharge near the extraction-channel end. For a given extraction voltage, two broad plasma resonances in the source output were often observed as the magnetic field was increased. The source was operated at the lower-resonance field value of about 50 G. The ion beam was accelerated to the desired final energy using a series of five cylinder lenses empirically adjusted for optimal beam focusing.

The 60° magnetic ion-beam mass analyzer used

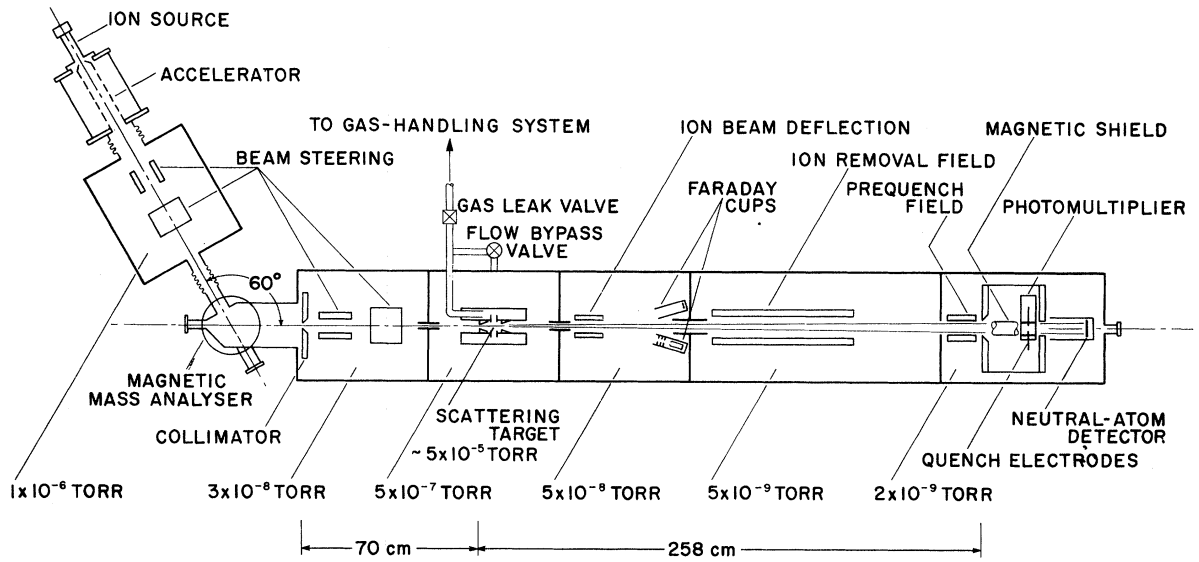


FIG. 1. Schematic diagram of the apparatus (not to scale). The beam entrance channel of the scattering cell is the second proton-beam collimating aperture. The exit channel of the cell is rectangular in cross section, as are the differential pumping conductances between the target and the atom detectors. The detectors are translatable, permitting studies of angular distributions. Typical operating pressures are indicated, for the proton-beam on and gas in the scattering cell.

a *C*-yoke magnet possessing 15-cm circular pole pieces and a 5-cm gap. The magnet exit aperture was the first of two 0.127-cm diameter ion-beam collimators that were separated by a distance of about 70 cm. The mass peaks corresponding to different hydrogen ions in the beam were completely resolved.

Radio-frequency discharge ion sources usually have inherent energy spreads between 20 and 500 eV, depending on design and operating parameters.[10] Most investigators have found the energy spread of the Thoneman source to be around 100 eV. In the present experiment, the shape of the proton mass peak was determined by varying the mass-analyzer magnetic field; the width of the peak yielded information on the beam energy spread. The energy calibration of the mass-analyzer scans was determined from the shifts in the mass spectrum (as a function of analyzer magnetic field) produced when the accelerator voltage was changed by a known amount. The total width of a mass peak in an analyzer scan was composed of partial widths due to the true beam energy spread, the analyzer momentum resolution, and the finite beam size. The observed total width at half-maximum was taken as an upper bound on the beam energy spread. A typical analyzer scan over the proton mass peak was found to contain a principal maximum with an energy width of at most 100 eV. At an energy of about 125 eV below the principal maximum, a small partially resolved second maximum was observed; the magnitude of this secondary maximum was never found to be more than about 3% of the principal one. Cross-section data were taken with the analyzer set at the peak of the large maximum; contamination from the apparent lower-energy beam component was then less than 1%.

In the present experiment, the uncertainty in the beam energy is just the uncertainty in the mean ion energy as extracted from the ion source. For the Thoneman radio-frequency source the mean ion energy has always been found to be from 50 to 400 eV higher than the extraction voltage,[11,12] because of the existence of a plasma potential. A plasma potential of 200 eV was assumed in the present experiment; the uncertainty in the beam energy was then about 0.2 keV.

When the electric deflection fields along the beam path were turned off, the proton beam traveled the length of the apparatus, where it could be collected in a Faraday cup mounted on the translatable detector assembly. A 0.13-cm diameter aperture was placed in front of the cup on the motion translator, and the detector assembly was scanned over the proton beam. The beam profile was found to possess the 0.09° full width at half-maximum predicted by collimation geometry. The edges of the profile dropped sharply, the full width at 0.1% of maximum intensity being

0.24°.

The Faraday-cup assembly used for precision ion-current measurements is shown in Fig. 2. Suppression of secondary electron losses from the beam collection surface was achieved through the use of deep-cup geometry, electron reflection electrodes, and cup biasing. The front aperture plate shown in the figure was interchangeable with other plates possessing slits or holes of different sizes. The third aperture plate was biased negative by about 150 V. The cup itself was biased about 45 V positive and possessed a slanted beam-collection surface in an attempt to minimize secondary ion losses.[13] An indication of the secondary-electron suppression capability of the Faraday-cup assembly was that it measured a neutral beam of intensity $I_0$ as an apparent negative ion beam of intensity $1.1\times10^{-3}I_0$.

### C. The Scattering Target

Figure 2 schematically shows the target system. The target gas to be used was stored in a gas ballast bottle at a pressure near 30 Torr. The ballast bottle pressure was measured with a capacitance manometer (MKS Model 77) referenced against a vacuum of less than $10^{-8}$ Torr. The calibration of the capacitance manometer at 30 Torr was checked with a mercury U-tube manometer. Target gas flow was controlled by a Varian bakeable gas metering valve. A Schulz-Phelps ion gauge (type W-7676) monitored the pressure at the output of the metering valve. The two methods used for determining the target thickness involved the measurement of gas flows. The principal components of the flowmeter were the ballast bottle, the capacitance manometer, and an adjustable volume element connected as part of the ballast volume. The target gas flow could be bypassed around the scattering cell.

The region containing the target gas was 1.10 cm in diameter and 4.3 cm in length. The differential pumping conductances at the ends of the target region were tapered beam channels, 2.54 cm long. The beam-entrance channel was of circular cross section and possessed a sharp front edge 0.127 cm in diameter; the beam exit channel was rectangular in cross section and had a sharp front edge with a horizontal dimension of 0.203 cm and a vertical dimension of 1.015 cm.

The scattering-cell beam-entrance channel was used as the second incident proton-beam collimator. This collimator and other scattering cell surfaces near the beam did not exhibit surface-charging effects.[14]

Considerable attention was given to the spatial definition of the scattering region. The general requirement of high differential pumping conflicted with the need for complete transmission of fast scattered beam particles through the scattering-cell exit channel. A well-defined scattering center was considered highly desirable; this implied that the target-to-detector separation was to be much greater than the target length. A 9-in. diffusion-pumping column was used on the target section of the vacuum system. Nevertheless, scattering due to target gas outside the target region and to vacuum system outgassing was not always negligible.

A gas-flow bypass technique was used to directly measure the amount of scattering occurring outside of the target. The basic idea involved is that background gas signals depend only to a small extent upon whether or not the gas flow into the apparatus actually passes through the scattering cell. The scattered atom signal obtained when the gas flow is directly introduced into the target vacuum pumping chamber should be subtracted as a correction from that signal obtained when the flow is through the scattering cell. The "difference signal" so obtained is due to scattering from an effective target composed of gas inside of the cell plus a small contribution from the atomic beam leaving the cell.

The gas-handling system of Fig. 3 could be operated in two states, depending on whether the high-conductance gas bypass valve was open or closed. In the latter or "gas-in" state, the scattering target arising from a gas flow $Q$ had a thickness

$$\Pi = P_c L_c + P_s(L_s - L_c) = \Pi_c + \Pi_b, \qquad (1)$$

where $L_C$, $L_S$ and $P_C$, $P_S$ are the lengths and pressures of the scattering cell and target pumping chamber, respectively. In the "gas-bypass" state the scattering target thickness was $\Pi' = P_S' L_S$ and arose from a flow $Q'$. The quantity $\Pi - \Pi'$

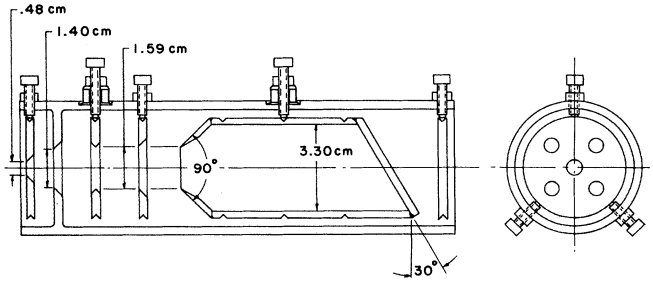


FIG. 2. Design of the high-precision Faraday-cup assembly. All electrostatic elements were shielded from the outside environment. Each element was aligned by three or more thumbscrews. Thumbscrews for ungrounded elements were either mounted in ceramic-to-metal electrical feedthroughs, or they possessed quartz tips. The front element was a removable aperture which determined the beam acceptance. The drawing is to scale.

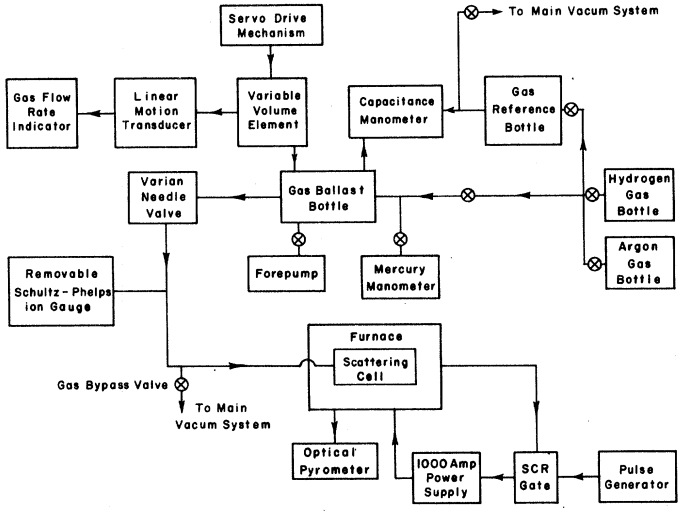


FIG. 3. Schematic diagram of the gas handling system. From the ballast bottle, gas flowed through the needle valve into the scattering cell. The capacitance manometer sensed the instantaneous drop in ballast bottle pressure produced by the flow. This pressure was held constant by continuous reduction of the ballast bottle volume through adjustment of the variable volume element. The rate of change in volume was a measure of the gas flow rate. The gas-bypass valve was used in measuring background-gas scattering corrections. The scattering cell could be heated in the furnace described in Ref. 16.

differs from $\Pi_c$ by a small amount:

$$(\Pi - \Pi')/\Pi_c = 1 - (\Pi' - \Pi_b)/\Pi_c = 1 - \delta, \qquad (2)$$

where the fractional error $\delta$ is

$$\delta = \frac{P'_s L_s - P_s(L_s - L_c)}{P_c L_c} = \left[1 + \frac{L_s}{L_c}\left(\frac{P'_s}{P_s} - 1\right)\right]\frac{P_s}{P_c}. \qquad (3)$$

If the speed of the target-chamber diffusion pump is independent of target state, $P'_s/P_s$ equals $Q'/Q$. We thus obtain

$$\delta = \left[1 + \frac{L_s}{L_c}\left(\frac{Q'}{Q} - 1\right)\right]\frac{P_s}{P_c}. \qquad (4)$$

The nonzero value $\delta = 0.023 \pm 0.008$ necessitated a small correction to the cross-section values obtained from the ("gas-in" minus "gas-bypass") difference scattering signals.

The first and more direct method for determining the target thickness was due to the relationship

$$\Pi_c(\text{molecules/Å}^2) = 3.30 P_c L_c, \qquad (5)$$

where $P_c$ is the pressure inside the cell in Torr and $L_c$ is the effective length of the scattering region in cm; $L_c$ contains a correction for the gas in the differential pumping channels. The quantity $P_c$ is determined from the cell conductance $C_c$ and the target gas flow $Q$ using the formula

$$Q = C_c P_c (1 - P_s/P_c).$$

The molecular flow conductance $C_c$ was estimated using formulas from Lyubitov[17] to be $(0.33 \pm 0.12)(T/M)^{1/2}$ liters/sec, where $T$ is the cell temperature in degrees Kelvin and $M$ is the molecular weight of the target gas. The remaining quantity to be determined was the gas flow rate $Q$.

The operation of the constant-pressure gas flowmeter (see Fig. 3) was similar to that of Haywood and Jepsen.[18] First both sides of the capacitance manometer were filled to a pressure near 30 Torr. The reference side of the manometer was then sealed off and the ballast side evacuated. This permitted measurement of the reference pressure $P_R$. The ballast bottle was then refilled until the manometer read zero. As gas flowed into the scattering target, the ballast pressure $P_0$ was held constant and equal to $P_R$ by reducing the ballast volume. The variable volume element consisted of a rod inserted through an O ring into the ballast volume and driven by a precision micrometer. The flow rate under these conditions was given by

$$Q = P_R dV/dt = P_R A dL/dt,$$

where $A$ is the cross-sectional area of the rod and $dL/dt$ is the rate at which the length of rod must be introduced into the ballast volume in order that $P_0 = P_R$. The quantity $dL/dt$ was measured throughout the taking of a data point. Its magnitude was determined from the slope of a straight-line least-squares fit to the values of $L(t)$.

The magnitude of $P_R$ was chosen so that thermal ballast-pressure fluctuations and gas-handling system outgassing were both negligible effects. The use of equal gas pressures in the two sides of the capacitance manometer reduced to very small values the apparent (but nonexistent) flow rate caused by room-temperature changes. Flow rates between $10^{-5}$ and $10^{-3}$ Torr liter per second were measured to an accuracy of $\pm \frac{1}{2}\%$.[19]

Prepurified grade gases were used in the gas-handling system. The background pressure in the ballast bottle when evacuated was $10^{-2}$ Torr. The use of a palladium leak for hydrogen did not affect the results. The target purity was believed to be better than 99%.

The principal uncertainties in $\Pi_C$ as determined

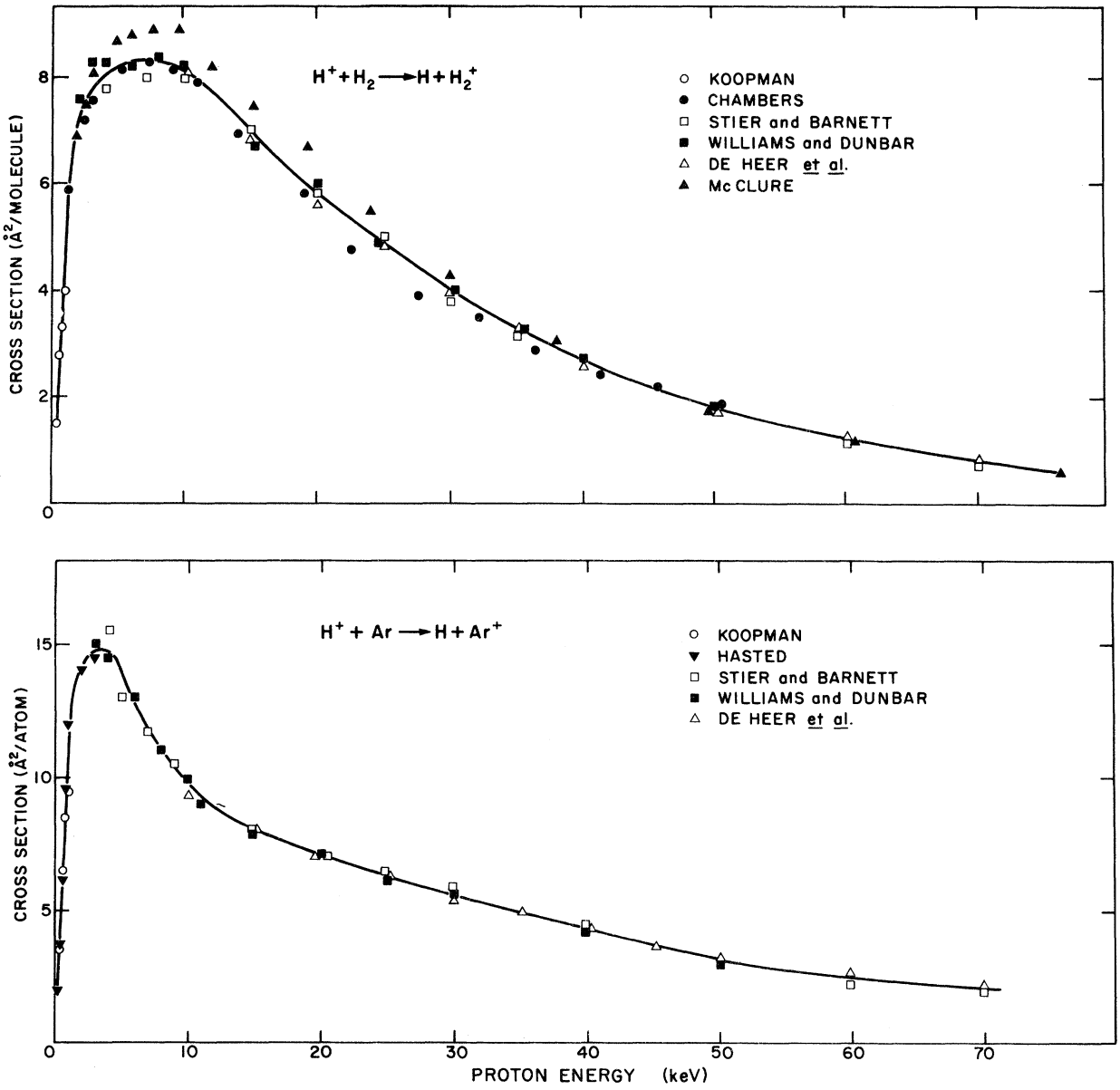


FIG. 4. Cross sections for total charge transfer considered for the second method of target density determination. (a) $H^+ + Ar$; (b) $H^+ + H_2$. Each set of data represents an independent absolute cross section measurement, except for that of Williams and Dunbar. Their results were normalized to those of Stier and Barnett at 10 keV.

above are those associated with the values of $C_c$ and $L_c$. The estimated over-all uncertainty in $\Pi_c$ determined by this first method was ±40%.

The second method of target-thickness determination is believed to be more accurate. In this calibration method, $\Pi - \Pi'$ is related to known cross-section values $\sigma_{10}(\mathrm{Ar})$ for total charge transfer. The intensity of the total fast atom beam is the basic measured quantity.

The absolute magnitudes of total charge-transfer cross sections in the keV energy range have been determined by many investigators. Figure 4 shows recent data[20] for $H_2$ and Ar, two of the most-studied target gases. Agreement between investigators is unusually good for $H^+ + Ar$. This is probably due to a number of factors, e.g., the cross section is quite large, differential pumping is relatively good for heavy gases, and the measurement of pressures is often less prone to systematic error for inert gases as compared to molecular gases such as $H_2$. Thus the values for $\sigma_{10}(\mathrm{Ar})$ were chosen as the basis for the second method of target-thickness determination. It is felt that the absolute magnitude of $\sigma_{10}(\mathrm{Ar})$ is presently known to within ±5% in the energy range between 7 and 70 keV, and to within ±10% from 2 to 7 keV.

The determination of target thickness for $H_2$ as a target gas was based on $\sigma_{10}(\mathrm{Ar})$ and gas-flow measurements. The value of $\Pi_c(\mathrm{H_2})$ arising from $Q(\mathrm{H_2})$ is obtained from a value of $\Pi_c(\mathrm{Ar})$ arising from $Q(\mathrm{Ar})$. The necessary relationship is

$$\frac{\Pi_c(\mathrm{H_2})}{\Pi_c(\mathrm{Ar})} = \frac{Q(\mathrm{H_2})}{Q(\mathrm{Ar})}\left(\frac{M_{\mathrm{Ar}}}{M_{\mathrm{H_2}}}\right)^{\frac{1}{2}}, \tag{6}$$

which follows from the fact that a molecular-flow conductance depends on gas type only through the velocity factor.

The relationship between $\Pi_c(\mathrm{Ar})$ and $\sigma_{10}(\mathrm{Ar})$ at sufficiently low values of $\Pi_c$ is

$$I^0 = I^+ \Pi_c(\mathrm{Ar})\sigma_{10}(\mathrm{Ar}), \tag{7}$$

where $I^+$ is the incident proton beam intensity and $I^0$ is the intensity of the neutral-atom beam produced by charge transfer. The measurement of $I^+$ was made to better than 1% accuracy using a Faraday-cup assembly of the type already described.

The measurement of $I^0$ was more complicated. The neutral-atom detector was a secondary-electron emission device composed of a 3.7-cm diameter stainless-steel disc located near the bottom of a metal cup 5 cm in diameter by 20 cm long. The cup was biased 300-V positive relative to the disc, thus collecting all secondary electrons emitted when the fast-atom beam was stopped on the disc. The number of secondary electrons per incident particle could not be measured for incident fast atoms, but was easily measured for incident protons. The question thus arose as to the relationship between the secondary electron coefficients $\gamma^+$ and $\gamma^0$ for incident protons and hydrogen atoms, respectively.

At quite low beam-particle velocities, the principal secondary-electron ejection mechanism available is known to be an Auger-effect ion neutralization process called potential emission.[21] Such a process does not occur for incident neutral atoms. Thus for beam energies below ~100 eV, $\gamma^0$ differs from $\gamma^+$ by a large amount. As the beam energy is increased, the probability for potential emission reaches a maximum and then decreases because the beam particle does not spend sufficient time at the surface for an Auger transition to occur. However, another mechanism becomes important as high momentum-transfer collisions of the beam particle with the lattice become probable. The resulting kinetic emission of secondary electrons increases with energy up to 10 or 20 keV and then tends to be constant.[21] As an impinging neutral atom is quickly stripped of its electron at the metal's surface, kinetic emission is essentially independent of the charge state of the beam particle.

Barnett, Stier, and Evans[22] and Chambers[23] have directly measured both $\gamma^0$ and $\gamma^+$ for nickel and beryllium-copper surfaces, respectively. The results of these investigators indicate that

$$\gamma^0/\gamma^+ = 1.11 + 0.001E \ (\mathrm{keV})$$

over the energy range presently used. Thus potential emission appears to be quite unimportant for the deeply penetrating protons and hydrogen atoms used in the present study.

The quantity $\gamma^+$ was measured for the present neutral-atom detector and was found to rise from a value of 2.2 at 2 keV to a peak value of 4.0 at 15 keV. The value of $\gamma^+$ then decreased to 3.7 at 25 keV and remained constant at $3.7 \pm 0.3$ for energies between 25 and 70 keV. The quantity $\gamma^0$ was therefore taken to be $4.1 \pm 0.3$ above 25 keV.

The two methods of determining $\Pi_c$ were simultaneously used in those runs involving beam energies above 25 keV. Agreement between the methods was always within 20%.

### D. Metastable Atom Detection

A sketch of the assembly used in fast-atom detection is shown in Fig. 5. The atom beam first passed through an interchangeable entrance aperture (or slit, when desired) and then through a grounded tubular electromagnetic shield before being subjected to the metastable quenching field produced by wire electrodes. The Ly $\alpha$ photon emission was observed with a resistance-strip photomultiplier (Bendix model M-306-1) possess-

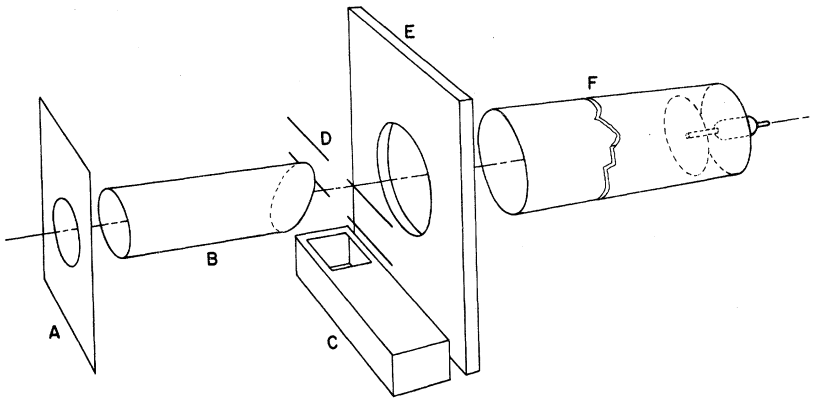


FIG. 5. The principal components of the detector assembly. The interchangeable aperture plate is indicated as A; the metastable quenching field wires as D; the Bendix photomultiplier as C; and the neutral atom secondary emission detector as F. The iron tube B eliminated the effects of photomultiplier fringe field quenching outside the view of the cathode. All components were contained inside an electrostatic shielding box and were mounted on the translatable slide E.

ing a smooth-surfaced tungsten cathode. As already described, the entire atom beam was stopped by the beam collection plate of a deep, backward-biased Faraday cup.

The quenching-field electrodes normally used consisted of opposing pairs of wires separated by a gap of 1.9 cm. The voltages on the electrodes located on the two sides of the beam were $+\frac{1}{2}V_q$ and $-\frac{1}{2}V_q$, respectively, with respect to the ground.

The photomultiplier used was a crossed electric and magnetic field device possessing a continuous tin oxide electron-multipler dynode surface.[24,25] Major advantages associated with this device were its over-all stability and very low dark counting rate ($\lesssim 10$ counts per minute) at a detection chamber vacuum of $< 10^{-8}$ Torr. A disadvantage lay in its fringe magnetic field, which can motionally quench H(2$s$) via the effective electric field $\vec{v}\times\vec{B}$.

The three components of the multiplier fringe magnetic field were measured at different points along the beam. The distance between the beam axis and the photocathode was 3.8 cm. Without the iron electromagnetic shielding tube shown in Fig. 5, the transverse magnetic field possessed a maximum of 45 G at the edge of multiplier structure, and decreased slowly to values of about 10 G for a distance of 10 cm in front of the multiplier. The introduction of the iron tube reduced these fields to less than 0.2 G, thus decreasing motional quenching in front of the Ly-$\alpha$ observation region to a negligible amount. Field measurements verified that the tube did not significantly alter the magnetic field inside the photomultiplier. A transverse magnetic field in the Ly-$\alpha$ observation region remained. The calculated H(2$s$) quenching due to this field reached 20% at the high end of the energy range. The problems associated with this quenching were alleviated by means of an H(2$s$) prequenching technique, described below.

In the absence of electric and magnetic fringe-field effects there are two equivalent definitions of the metastable atom signal. One may pass the metastable beam into the quenching region, and define the signal as the difference in photomultiplier counting rates for quench field on and then off. The magnitude of the field must be chosen so as to quench all metastables in the beam, i.e., a saturation of the difference signal must be achieved. The presence of an extraneous magnetic field in the quench region complicates this first definition of the metastable signal, for the motional part of the net quench field cannot be turned off.

The prequenching technique avoided the motional field problem. In this second procedure for defining the signal, the quenching field was held constant while the metastable beam could be quenched before entering the detector chamber. The metastable signal was then defined as the difference in counting rates for the prequench electric field first off and then on, under the conditions that both quench and prequench voltages be high enough to saturate the difference signal. This procedure was adopted for the present measurements. The effect of photomultipler fringe magnetic-field quenching was then merely an alteration of the spatial distribution of quenching radiation in the Ly $\alpha$ observation region.

The dependence of the metastable atom signal $B$ on quenching voltage $V_q$ was studied in detail for various energies. The magnetic-field quench-

ing effect was observable, as it was responsible for differences between the field dependences of the quenching for the two possible polarities for $V_q$. The dependence of $B$ on $V_q$ varied as

$$1 - \exp[-k(V_q - V_0)^2]$$

to within ± 10%, where $V_0$ was 80 V at 15 keV. The saturated value of $B$ was independent of the sign of $V_q$ to within ± 2%. At 15 keV, $B$ was 98% saturated for $V_q$ = 1600 V. Values of $V_q$ up to 3.5 kV could be maintained without difficulty. In practice, the value of $V_q$ chosen for cross-section measurement was determined by observing saturation and then reducing the field to the 95% quenching level; the data were corrected accordingly.

The prequenching electric field (see Fig. 1) was provided by two parallel plates. The metastable signal was observed to vary with prequench voltage $V_{pq}$ and beam energy $E$ according to

$$\exp(-k'V_{pq}^2 E^{-1/2}),$$

as predicted by theory.[26] A calculated value of $k'$ was in excellent agreement with that determined from experimental curves.

The variation of metastable signal with ion removal voltage was also found to vary as

$$\exp(-k''V_I^2 E^{-1/2}),$$

given that the voltage was sufficiently large to remove all ions. A value of $k''$ was determined from the experimental curves, and used to compute the ion-removal field quenching loss.

The basic problem associated with metastable atom detection was the determination of the overall efficiency $\eta^*$, defined as the probability that a photomultiplier count be registered if a fast metastable atom leaves the scattering cell. If $B$ is the difference counting rate (prequench off minus prequench on) and $N^*(0)$ is the H(2s) flux leaving the target, then $\eta^* = B/N^*(0)$. This quantity depends on several factors: The ion-removal field quenching loss $Q_I$; the details of the detector quenching field $F$; a Ly $\alpha$ collection solid-angle factor $\Omega$; the photomultiplier quantum efficiency; and whatever signal losses occur in the pulse-handling electronics. The formulae used to calculate $\eta^*$ are discussed in the Appendix.

The photoelectric yield $\eta_w$ (number of electrons emitted per incident photon) for Ly $\alpha$ normally incident on tungsten has been a subject of considerable study.[27–30] The spread in published values lies between 0.016 and 0.030; the lower values are obtained for the cleaner surfaces.[30] We therefore take $\eta_w = 0.023 \pm 0.017$, a reasonable value for a degreased but otherwise untreated tungsten photocathode operated in a vacuum of less than $10^{-8}$ Torr. The angular dependence $\eta_p$ of $\eta_w$ has been studied[31] and is a small effect at 1216 Å.

Spatial dependence in the magnetic electron-multiplier photoelectron collection efficiency $\eta_c$ has been studied for the Bendix model M-303.[32] The situation is expected to be very similar for the Model 306-1 presently used, once the factor-of-two increase in the magnetic field used in the M-306-1 is taken into account. This quantity is dependent on the voltages applied on the multiplier. The Ly-$\alpha$ counting rate was found to be maximized for grid-cathode voltages between 800 and 900 V, in agreement with other investigations.[33] At the corresponding voltage of about 200 V for the M-303, $\eta_c$ is fairly uniform.[32] This spatial dependence of $\eta_c$ for the M-303 (near the cathode) was taken to apply in the present case. A calculation of the trochoidal electron trajectories in the multiplier indicated that a mean value of $\eta_c$ unequal to one was caused by electron loss due to passage outside the grid. The effect of this loss was to result in a mean value of $\eta_c$ of $0.7 \pm 0.2$.

The photomultiplier grid transparency $\eta_T$ was $0.90 \pm 0.02$. The number of counts lost below the level determined by a discriminator in the pulse-handling electronics was estimated from the derivative of the curve of counting rate versus discriminator voltage. The electronics efficiency $\eta_e$ so determined was $0.80 \pm 0.05$.

The value of $\eta^*$ determined from Eq. (13) of the Appendix was $1.1 \times 10^{-4}$ counts per metastable atom. The uncertainty in this number is estimated to be ± 55%.

### E. The Elimination of Possible Systematic Errors

The principal sources of systematic error not already discussed are mechanisms through which extraneous metastable-atom beam gain or loss can occur. The gain mechanisms include multiple collisions, scattering by background gas, and collisions with surfaces. The loss mechanisms include all of these plus any effects due to stray electric or magnetic fields.

The probability for multiple scattering in the (background-gas corrected) target was reduced to low levels through the use of sufficiently low scattering-cell pressures. The closely linear dependence of the metastable-atom signal on target-gas flow rate was studied for both gases at various energies. All cross-section data were taken at gas flow rates below those producing a nonlinear contribution to the pressure dependence of 4%.

Stray electric fields inside the apparatus were guarded against by the shielding of all insulating surfaces from the beam. All electrical cables were also shielded. The ultrahigh base vacuum achieved through the use of mercury diffusion pumping made charged insulating surface layers unlikely.

The apparatus was made of nonmagnetic materi-

als except for the photomultiplier and mass analyzer. Measurements of the magnetic field along the beam axis showed that the metastable-atom beam was exposed to no magnetic fields other than the fringe field of the photomultiplier and the earth's magnetic field. The ion beam in the collimation region was exposed to both a fringe field from the mass-analyzer magnet and the earth's magnetic field. The effect of these latter fields was to necessitate a small amount of electrostatic beam steering in the collimation region. This was done using plane-parallel deflection plates. The voltages on these plates were adjusted so as to maximize the neutral-atom beam signal received at the detector end of the apparatus. This insured that the atom beam produced by scattering in the target proper was correctly directed. The steering voltages used were so small that defocusing of the ion beam was insignificant.

The angular distribution of the scattered fast-atom beam was studied. A horizontal slit was placed in front of the fast particle detectors mounted on the vertical motion translator. The slit possessed dimensions $0.17 \times 1.26$ cm, and was 258 cm from the center of the scattering target. The metastable-atom and neutral-atom signals (gas in minus gas bypass) were simultaneously recorded as the detector assembly (with slit) was scanned across the beam. The scans were taken out as far as the 1% signal level, except below 5 keV, where the signal was sometimes lost in the background at the 5 to 10% level.

At energies above 20 keV, both metastable and total neutral-atom angular distributions were found to be essentially the same as the incident proton distribution, the added angular spread being less than 0.01°. At lower energies, both neutral-beam distributions broadened as energy was reduced; the broadening of the metastable beam was somewhat greater than that for the total neutral beam. The broadest distributions were found for $H_2$ at 3 keV; here the neutral-atom beam pattern possessed a full width at 10% of maximum of 0.13°. The corresponding value for the metastable beam was 0.17°.

The observations made on the angular spreads are in general agreement with those for total neutral atoms by McClure[20] and by Wittkower, Rose, Bastide, and Brooks.[34] The presently observed differences between the metastable and total-neutral distributions are in themselves interesting; this matter might be pursued with higher angular resolution and lower energy beams.

The scattering cell described in Sec. B transmitted all fast scattered particles that had undergone deflections out of the incident beam of no more than $0.18 \pm 0.01$°. The optical alignment procedure used reproducibly defined the beam axis to within ± 0.006°. Motion of the apparatus during chamber evacuation was measured to distort the beam axis by less than 0.005°. Every aperture beyond the scattering-cell exit slit transmitted all particles leaving the scattering cell. Hence the loss of scattered beam particles was insignificant, except below 5 keV where it reached values perhaps as high as 20%. Corrections based on the measured angular distributions were made to the

TABLE I. Measured cross-section values for $\sigma_{2s}(H_2)$ and $\sigma_{2s}(Ar)$. The stated uncertainties are for the energy dependence. The absolute magnitude of $\sigma_{2s}(Ar)$ is best obtained by normalization to $0.29 \pm 0.07$ Å$^2$ at 20 keV (see text).

| Proton energy (keV) | $\sigma_{2s}(H_2)$ (Å$^2$) | $\sigma_{2s}(Ar)$ (Å$^2$) |
|---|---|---|
| $2.0 \pm 0.2$ | $0.03 \pm 0.03$ | $0.10 \pm 0.03$ |
| 4.0 | $0.056 \pm 0.013$ | $0.086 \pm 0.016$ |
| 6.0 | $0.081 \pm 0.010$ | $0.067 \pm 0.013$ |
| 8.0 | $0.086 \pm 0.009$ | $0.135 \pm 0.020$ |
| 10.0 | $0.107 \pm 0.017$ | $0.21 \pm 0.025$ |
| 15.0 | $0.162 \pm 0.022$ | $0.31 \pm 0.020$ |
| 20.0 | $0.23 \pm 0.017$ | $0.31 \pm 0.025$ |
| 30.0 | $0.27 \pm 0.020$ | $0.28 \pm 0.030$ |
| 50.0 | $0.180 \pm 0.019$ | $0.182 \pm 0.022$ |
| 70.0 | $0.091 \pm 0.009$ | $0.125 \pm 0.015$ |

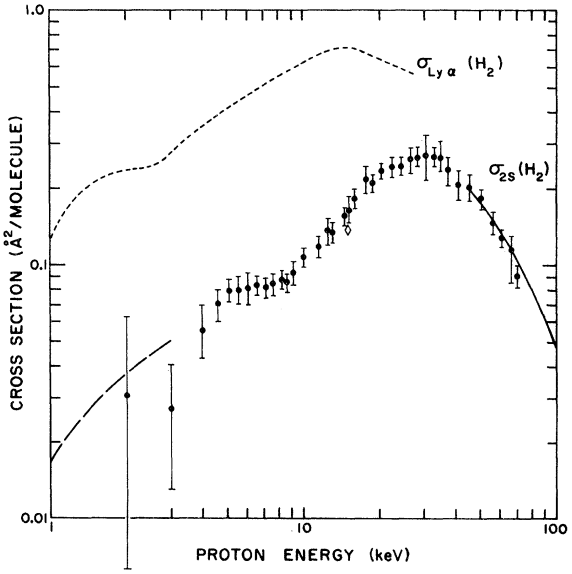


FIG. 6. The cross section $\sigma_{2s}(H_2)$ for the process $H^+ + H_2 \rightarrow H(2s) + H_2^+$. ● Present data; —— Ryding, Wittkower, and Gilbody, normalized to the present value at 50 keV; --- Donnally, Richard and Sawyer; ◊ Sellin. The error bars contain all sources of uncertainty except for an uncertainty of ± 55% in the cross-section scale associated with the efficiency for H(2s) detection. The cross section $\sigma_{Ly\,\alpha}(H_2)$ for the process $H^+ + H_2 \rightarrow Ly\ \alpha$ as measured by Van Zyl, Jaecks, Pretzer, and Geballe is shown for comparison.

cross-section values at the lowest energies.

The collision of fast protons or hydrogen atoms with metallic surfaces is known to produce sizeable amounts of light.[35,36] Definite evidence of this was found in the present experiments. It was necessary to stop the deflected ions in the ion-removal region by collisions at normal incidence with a surface not viewed by the detector assembly. In addition, a good portion of the background light signal observed with the prequench voltage on was due to the stopping of the fast neutral atoms at the neutral detector collection plate. Background signals of this type were eliminated through definition of the metastable signal as prequench on minus prequench off.

## III. RESULTS AND DISCUSSION

The results of the experiment for $H^+ + H_2$ are shown in Fig. 6. (See also Table I.) The error bars shown include all uncertainties affecting the energy dependence of the cross section. The error in the absolute value of the cross section must include the additional ±55% uncertainty in the metastable-atom detection efficiency $\eta^*$. The larger error bars below 5 keV arise from relatively poor signal-to-background ratios coupled with some uncertainty in the fraction of metastables lost at scattering angles greater than 0.18°.

The original work on $\sigma_{2s}(H_2)$ of Madansky and Owen[1] indicated that the cross section[37] was at least 0.01 Å$^2$ at 10 keV. Following their work, experiments were conducted by Christofori and co-workers between 8 and 40 keV.[2] They used an incident hydrogen-ion beam (of mixed composition) obtained directly from a gas discharge; the external quenching method was employed under conditions of small solid-angle acceptance. Their cross section possessed a maximum near 25 keV, and a magnitude of 0.025 Å$^2$ at 15 keV. This was in marked disagreement with a value of 0.2 Å$^2$ obtained by Sellin[2] at the single energy of 15 keV. The present data supports Sellin's work.[38]

Figure 6 shows smooth curves drawn through the data of Ryding, Wittkower, and Gilbody[4] obtained above 43 keV, and the preliminary data of Donnally, Richard, and Sawyer[39] obtained below 3 keV. The relative cross-section data of the former group has been normalized to the present value at 50 keV. Within experimental error, all data presented in Fig. 6 are in agreement.

The cross section $\sigma_{2s}(H_2)$ is found to have a principal maximum at 30 keV and secondary structure near 6.5 keV. The secondary structure lies near the maximum in the total charge-transfer cross section $\sigma_{10}(H_2)$ which occurs in the region 7 to 9 keV.[20] This suggests that the two-step process

$$H^+ + H_2 \rightarrow H(1s) + H_2^+ \rightarrow H(2s) + H_2^+$$

may be involved in some meaningful way. The importance of intermediate states has already been indicated in the cases of $\sigma_{2s}(He)$ and $\sigma_{2s}(Ne)$, both experimentally[5,7] and theoretically.[40] On the other hand, the cross section for total Ly $\alpha$ production in $H^+$-$H_2$ collisions (see Fig. 6) has been found[41] to possess a similar low-energy structure at about 2 keV, considerably below the maximum in $\sigma_{10}(H_2)$. Thus the relevance of a simple two-step process is, in general, uncertain; the observed partially resolved shape resonance may well be due to some other mechanism.

The presently obtained external-quenching data for $H^+ + Ar$ is presented in Fig. 7. (See also Table I.) The error bars have the same meaning as for $H^+ + H_2$. The low-energy maximum in $\sigma_{2s}(Ar)$ evident in the earlier internal-quenching data has been confirmed. As in $H_2$, this maximum occurs near the peak of the total charge-transfer cross section; an interpretation in terms of two-step processes is possible.

The agreement of the present data with the absolute internal-quenching measurements of Andreev, Ankudinov, and Bobashev[6] is excellent for energies between 10 and 30 keV, as is the agreement with the low-energy data.[39] Within experimental errors, the value of the cross section $\sigma_{2s}(Ar)$ obtained by Jaecks, Van Zyl, and Geballe[5] at any one energy is in agreement with the corresponding data point obtained here. There does however exist some apparent disagreement in the energy dependence. This cannot be completely removed by either a shift in the energy scale or a multiplicative change in the cross-section scale. It can be concluded from the argon data of Fig. 7 that any differences in the cross-section values obtained using internal and external quenching are

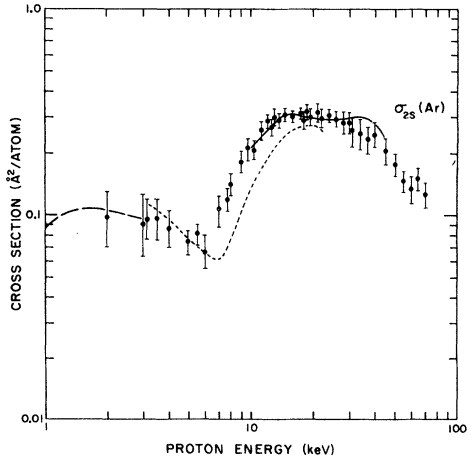


FIG. 7. The cross section $\sigma_{2s}(Ar)$ for the process $H^+ + Ar \rightarrow H(2s) + Ar^+$. ● Present data; —— Andreev, Ankudinov and Bobashev; .... Jaecks, Van Zyl, and Geballe; --- Donnally, Richard, and Sawyer. The error bars have the same meaning as in Fig. 6.

at present masked by systematic errors and are small.

An important aspect of the three experiments on argon is that they constitute almost-independent measurements of absolute cross-section values. The techniques used in each case were based upon accepted procedures for calibrating Ly-$\alpha$ detectors. The method employed by Andreev *et al.* (estimated error ± 20%) depended on the sensitivity of a windowless nitric oxide ionization chamber installed on their apparatus. The ionization efficiency of NO at Ly $\alpha$ has been extensively studied[42] and is believed known to within ± 5%. The data of Jaecks *et al.* (estimated error ± 50%) was taken using an iodine-vapor-filled photon counter with windows and an $O_2$ gas wavelength filter. Through measurements of the cross section for $e + H_2 \rightarrow$ Ly $\alpha$, the sensitivity of their detector can be related to the calibration of a different $I_2$ counter used by Brackman, Fite, and Hagen.[43] The latter compared the sensitivity of two counters of similar geometry, the one containing $I_2$ and the other containing NO. The present data is based on the photoelectric effect for tungsten, itself compared to the photo-ionization efficiency of NO and of the inert gases.[29,30]

Thus three relatively accurate determinations of absolute cross-section values for $\sigma_{2s}(\mathrm{Ar})$ are now available. The value $\sigma_{2s}(\mathrm{Ar}) = 0.29 \pm 0.07$ Å$^2$ at 20 keV should provide a good calibration point for future experiments.


## ACKNOWLEDGMENTS

I wish to thank Professor V. W. Hughes for his advice, encouragement, and support. The assistance of Dr. R. V. Krotkov in determining the initial design of the apparatus was greatly appreciated. The help of R. Molof during the taking of data is gratefully acknowledged.


## APPENDIX: THE H(2*s*) DETECTION EFFICIENCY

Let $z = 0$ denote the position of the target exit slit along the beam axis. We use cylindrical coordinates and, for simplicity, we assume axial symmetry. We also assume atom trajectories parallel to the $Z$ axis. Let $w(\rho, z)$ be the transition probability for the quenching of a metastable atom residing at the point$(\rho, z)$ along the beam. The loss of metastable atoms in the increment $dz$ becomes

$$dN^* = -w(\rho,z)N^*(\rho,z)dt = -w(\rho,z)N^*(\rho,z)dz/v \quad (8)$$

which implies that

$$N^*(\rho,z) = N^*(\rho,0)\exp[-v^{-1}\int_0^z w(\rho,z')dz'] . \quad (9)$$

Here $v$ is taken as the mean velocity of the initial proton beam; the spread in proton velocities and the momentum transfer in the collision are a small fraction of the mean velocity and are therefore ignored. Let $\eta(\rho, z)$ be the over-all efficiency of the detection system for detecting a quenched metastable atom at the point $(\rho, z)$. The increase $dB$ in a signal resulting from $dN^*$ is then

$$dB = [N^*(\rho,0)/v]\ \eta\ (\rho,z)w(\rho,z) \times \exp[-v^{-1}\int_0^z w(\rho,z')dz']dz . \quad (10)$$

The quantity $w(\rho, z)$ has contributions only from field quenching. Thus[26]

$$W(\rho,z) = \left\{\tau_{2p}\left[1+\left(\frac{2\xi(\rho,z)}{1-[1+\xi^2(\rho,z)]^{1/2}}\right)^2\right]\right\}^{-1} , \quad (11)$$

where $\tau_{2p}$ is the field-free lifetime of the $2p$ state of hydrogen, $\xi(\rho,z) = F(\rho,z)/475$, and $F(\rho,z)$ is the strength of the net electric field at the point $(\rho, z)$ in V/cm (for the prequench field off). When $F(\rho,z) \ll 475$ V/cm, $w(\rho,z) \approx \xi^2(\rho,z)\tau_{2p}^{-1}$.

We define the detection region as that region $z_1 \leq z \leq z_2$, wherein both $\eta(\rho, z)$ and the quenching field are nonzero. The geometry chosen in the experiment insured that $F(\rho, z)$ was significantly nonzero only in the ion removal and detection regions, and that these regions did not overlap. Assume $w(\rho, z)$ is independent of $\rho$ in the ion-removal region. In this case

$$\eta^*\int_0^a N^*(\rho,0)\rho d\rho \equiv \pi a^2 B = (Q_I/v)\int_0^a N^*(\rho,0)\int_{z_1}^{z_2}\eta(\rho,z)w(\rho,z) \times \exp[-v^{-1}\int_{z_1}^{z_2} w(\rho,z')dz']dz\,\rho d\rho, \quad (12)$$

where the ion-removal quenching loss $Q_I$ is a measured quantity, and $a$ is the beam radius.

Further evaluation of $B$ requires a detailed knowledge of $\eta(\rho, z)$ and $F(\rho, z)$ inside the detection region. The quantity $\eta(\rho, z)$ depends on $(\rho, z)$ for several reasons: (1) the spatial dependence of the photomultiplier photoelectron collection efficiency $\eta_c(\rho, z)$; (2) the small variation $\eta_p(\rho, z)$ of the mean photocathode quantum efficiency $\eta_w$ with incident photon direction; (3) the solid angle $\Omega(\rho, z)$ subtended by the cathode at the point $z$; (4) the transmission $\eta_T$ of the multiplier grid; and (5) the fraction $\eta_e$ of the multiplier output pulses actually counted. The quenching field $F(\rho, z)$ includes the contribution due to the photomultiplier fringe magnetic field.

Consider the limiting case of a uniform quenching field confined to a small region $\Delta z$ lying a

large distance $d$ from the photocathode. If constant values are taken for $\eta_c$ and $\eta_p$, then we obtain the usual result:

$$\eta^* \approx Q_I \eta_w \eta_p \eta_c \eta_T \eta_e \Omega (1 - e^{-w(F)\Delta z/v}). \quad (13)$$

This equation was a reasonably good approximation in the case of the present experiment, as was verified through numerical calculations based upon the more general expression.

Some numerical computations of $\eta^*$ were made for various possible quench field electrodes, including two apertures and two semiplanes with a gap in between. The dependence of the field on polar angle was included. Integrations over the finite diameter of the beam were performed using the actual beam distribution; the measurement of this distribution is discussed in Sec. D.

The calculations of $\eta^*$ included the effects of multiplier magnetic-field quenching; when the spatial distribution of the magnetic field was included, the result changed by about 4%. It was found that $\eta^*$ did not strongly depend on quench electrode type, given that, (1) the electrode spacing was a little larger than the beam diameter; (2) the electrode dimension along the beam direction was kept below 0.5 cm; and (3) the quench voltage was operated a little below the saturation value. These three conditions result in minimized quenching in front of the photocathode while simultaneously taking advantage of the $\exp(-kF^2)$ field dependence to maximize the quenching above the center of the cathode. The spread in values of $\eta^*$ under these conditions was ±20%, depending on the electrode configuration chosen.

---

*Research sponsored by the Air Force Office of Scientific Research, Office of Aerospace Research, United States Air Force under AFOSR Grant No. 41060.

[1]L. Madansky and G. E. Owen, Phys. Rev. Letters 2, 209 (1959).

[2]A. Cesati, F. Christofori, L. Colli, and P. G. Sona, Energia Nucl. (Milan) 13, 649 (1966). See also Phys. Letters 3, 62 (1962).

[3]I. A. Sellin, Phys. Rev. 136, A1245 (1964).

[4]G. Ryding, A. B. Wittkower, and H. B. Gilbody, Proc. Phys. Soc. (London) 89, 547 (1966).

[5]D. Jaecks, B. Van Zyl, and R. Geballe, Phys. Rev. 137, A340 (1965).

[6]E. P. Andreev, V. A. Ankudinov, and S. V. Bobashev, Zh. Eksperim. i Teor. Fiz. 50, 565 (1966) [English transl.: Soviet Phys. – JETP 23, 375 (1966)].

[7]V. Dose, Helv. Phys. Acta 39, 683 (1966).

[8]J. E. Bayfield, Phys. Rev. Letters 20, 1223 (1968).

[9]P. C. Thoneman, Progr. Nucl. Phys. 3, 219 (1953).

[10]M. D. Gabovich, Plasma Ion Sources (Kiev, Naukova Dumka, 1964). [English transl.: by U.S. Air Force Systems Command (Wright Patterson Air Force Base, Ohio)].

[11]C. J. Cook, O. Heinz, D. C. Lorentz, and J. R. Peterson, Rev. Sci. Instr. 33, 649 (1962).

[12]D. Blanc and A. Degeilh, J. Phys. Radium 22, 230 (1961).

[13]E. S. Chambers, Phys. Rev. 133, A1202 (1964).

[14]G. J. Lockwood, H. F. Helbig, and E. Everhart (see Ref. 15) found while studying $He^+$-He collisions that near or below energies of 1 keV an anomalous spreading of the incident ion beam occurred inside the target. They further found that heating of the target to 2000°K eliminated the effect, presumably because of surface charge neutralization through thermionic emission. The present scattering cell was made out of tungsten and could be heated to temperatures as high as 2600°K. See Ref. 16. A comparison of $H^+$-Ar data taken with the target first cold and then hot indicated that charged target-surface effects on both the incident proton beam and the scattered metastable atom beam were absent.

[15]G. J. Lockwood, H. F. Helbig, and E. Everhart, Phys. Rev. 132, 2078 (1961).

[16]J. E. Bayfield, Rev. Sci. Instr. (to be published).

[17]Yu N. Lyubitov, Molecular Flow in Vessels (Consultants Bureau, New York, 1967), Sec. 6.

[18]W. H. Hayward and R. L. Jepsen, Proceedings of the Ninth National Symposium of the American Vacuum Society, edited by G. H. Bancroft (The Macmillan Company, New York, 1959).

[19]The reproducibility of the flow measurements was about ± ½%. This determined the uncertainty in $Q$ as the factory calibration of the capacitance manometer was assumed. Comparison with a mercury manometer at 30 Torr showed the calibration accurate to within at least ± 2%.

[20]The data for $H^+ + Ar$ were taken from D. W. Koopman, Phys. Rev. 154, 79 (1967); P. M. Stier and C. F. Barnett, *ibid.* 103, 896 (1956); J. F. Williams and D. N. F. Dunbar *ibid.* 149, 62 (1966); J. B. Hasted, Proc. Roy. Soc. (London) A205, 421 (1951); and F. J. DeHeer, J. Schutten, and H. Moustafa, Physica 32, 1766 (1966). The above references also contain data for $H^+ + H_2$; the other data for this latter process are due to G. W. McClure, Phys. Rev. 148, 47 (1966); E. S. Chambers, University of California Radiation Laboratory Report No. 6987, 1965 (unpublished).

[21]M. Kaminsky, Atomic and Ionic Impact Phenomena on Metal Surfaces (Academic Press, Inc., New York, 1965), Chap. 12.

[22]C. F. Barnett, P. M. Stier, and G. E. Evans, Phys. Rev. 95, 307 (1954).

[23]E. S. Chambers, Phys. Rev. 133, A1202 (1964).

[24]L. Heroux and H. E. Hinteregger, Rev. Sci. Instr.

31, 280 (1960).
[25]G. W. Goodrich and W. C. Wiley, Rev. Sci. Instr. 32, 846 (1961).
[26]H. A. Bethe and E. Salpeter, Quantum Mechanics of One- and Two-Electron Atoms (Academic Press Inc., New York, 1951), Sec. 67.
[27]H. E. Hinteregger and K. Watanabe, J. Opt. Soc. Am. 43, 604 (1953).
[28]J. E. G. Wheaton, J. Opt. Soc. Am. 54, 1287 (1964).
[29]R. B. Cairns and J. A. R. Samson, J. Opt. Soc. Am. 56, 1568 (1966).
[30]K. Watanabe, F. M. Matsunaga, and R. B. Jackson, "Some Intensity Measurements in the Vacuum Ultraviolet," Physics Dept., University of Hawaii, 1964 (unpublished).
[31]L. Heroux, J. E. Manson, and H. E. Hinteregger, J. Opt. Soc. Am. 55, 103 (1965).
[32]L. A. Hall and H. E. Hinteregger, A. F. Cambridge Research Laboratories, Report No. AFCRL-TR-60-428, 1960 (unpublished).
[33]H. K. Holt and R. Krotkov, Phys. Rev. 144, 82 (1966).
[34]A. B. Wittkower, P. H. Rose, R. P. Bastide, and N. B. Brooks, Rev. Sci. Instr. 35, 1 (1964).
[35]A. A. Sterk, C. L. Marks, and W. P. Saylor, Phys. Rev. Letters 17, 1037 (1966).
[36]V. V. Gritsyna, T. S. Kijan, A. G. Koval, and J. M. Fogel, Physics Letters 27A, 292 (1968).
[37]All cross sections are in units of $Å^2$ per molecule.
[38]It should be noted that the measurements of $\sigma_{2s}$(He) presented in Refs. 5, 6, and 7 also are in disagreement with the helium data of Ref. 2.
[39]B. L. Donnally, T. Richard, and W. Sawyer, Bull. Am. Phys. Soc. 10, 85 (1965). Also B. L. Donnally, private communication.
[40]I. A. Poluektov and L. P. Presnyakov, Zh. Eksperim. i Teor. Fiz. 54, 120 (1968) [English transl.: Soviet Phys. – JETP 27, 67 (1968)].
[41]B. Van Zyl, D. Jaecks, D. Pretzer, and R. Geballe, Phys. Rev. 158, 29 (1967).
[42]K. Watanabe, F. M. Matsunaga, and H. Sakai, Appl. Opt. 6, 391 (1967).

PHYSICAL REVIEW VOLUME 182, NUMBER 1 5 JUNE 1969

# Formal Theory of Resonance Scattering*

Marvin H. Mittleman
*The City College of The City University of New York, New York*, 10031
(Received 27 December 1968)

A formal theory of resonances is presented in the Feshbach formalism with the use of more general projection operators and the relationship with other resonance formulations is clarified. The resonance position and true width are defined. They depend upon the background, or potential, scattering. An attempt is made to define the resonance state without using a "preconceived notion" of its structure. The attempt is not totally successful but the resultant equation is shown to be useful in obtaining corrections to other resonance formulations.

## I. INTRODUCTION

Phenomenological descriptions of resonances in the scattering of a particle by a bound group of particles have existed for some time.[1] It is only recently that any real attempt at an *a priori* calculation of the resonance parameters has been attempted.[2] There have been widely differing techniques applied to the problem of the calculation of the resonance state but the relationship between them is not completely clear. Indeed it will be shown that the definition of this resonance state is not unique.

The current description of resonances breaks them into at least two categories; the first, the closed channel, or Feshbach, resonances has a resonance state which is crudely describable as a particle bound to the target in an excited state which is energetically closed. The second category, open channel, shape, or potential resonances, is crudely describable as a particle bound to the target in the ground state or to an excited state which is energetically open. Characteristically the resonance of the first class usually occurs at an energy just below the energy of the closed channel with a narrow width while those of the second class appear at an energy just above the open-channel bound state with a much broader width. Many examples of closed-channel resonances are available in the case of electron-atom